BlendVLC

A cell-free VLC network architecture empowered by beamspot blending

Beysens, Jona; Wang, Qing; Van Den Abeele, Maxim; Pollin, Sofie

DOI
10.1109/INFOCOM42981.2021.9488727

Publication date
2021

Document Version
Final published version

Published in
INFOCOM 2021 - IEEE Conference on Computer Communications

BlendVLC: A Cell-free VLC Network Architecture Empowered by Beamspot Blending

Jona Beysens[1], Qing Wang[2], Maxim Van den Abeele[1] and Sofie Pollin[1]
[1]KU Leuven, Belgium [2]Delft University of Technology, Netherlands
Email: {jona.beysens, sofie.pollin}@kuleuven.be, maximvda123@gmail.com, qing.wang@tudelft.nl

IEEE INFOCOM 2021 - IEEE Conference on Computer Communications | 978-1-6654-0325-2/21/$31.00 ©2021 IEEE | DOI: 10.1109/INFOCOM42981.2021.9488727

***Abstract*—In visible light communication (VLC), the quality of communication is primarily dominated by line-of-sight links. To ensure an appropriate link quality anywhere, beamsteering has been proposed where transmitters (TXs) dynamically steer their beams to create *beamspots* on the users. However, these highly dynamic TXs face the beam tracking problem and result in highly variable illumination. In this work, we propose *BlendVLC*, a cell-free network architecture to improve the mobility robustness of users *by blending the beamspots from both steerable and fixed TXs.* We solve the beam tracking by designing a centimeter-level visible light positioning algorithm empowered by a neural network. Relying on this location information, we formulate and solve an optimization problem on the beamspot blending, and design a fast and scalable heuristic for large networks. We build a proof-of-concept testbed as well as a simulator to evaluate BlendVLC. We show that it achieves superior performance compared to denser networks with fully fixed TXs. For example, in a large-scale VLC network of 8 m x 4 m, BlendVLC improves the average system throughput by 30%, while only requiring *half the number of TXs*.**

***Index Terms*—Visible light communication, beamsteering, cell-free, mobility, positioning, tracking**

I. Introduction

Wireless networks are dominating our daily lives. By 2023, over 70% of the global population will have mobile connectivity and there will be 3.6 networked devices *per capita* [1]. To accommodate this increasing density in wireless devices, further advancements in communication technologies are required. Despite the continuous efforts spent on radio frequency (RF) technologies, they lack the sufficient RF spectrum to meet this ongoing and ever-expanding traffic demand [2].

Visible light communication (VLC) has attracted significant attention on complementing RF networks to provide reliable communication in ultra-dense scenarios. Due to the directivity of LED beams, VLC facilitates a high level of spatial reuse, allowing to create a network of atto-cells with densely deployed transmitters (TXs) [3]. *However, in mobile scenarios, a dense VLC network increases the deployment cost and leads to more frequent handover overhead, reducing mobility robustness.*

To reduce the density of TXs, steerable LED TXs have been proposed in which the direction of light beams can be adapted to always point to mobile users, also known as *beamsteering*. Using such steerable directional beams could maximize the signal strength and coverage area [4], [5]. Further, by lowering the semi-angles of LEDs, dynamic precise beamspots can be formed with minimal interference among the beams. However, *these works neglect the beam tracking problem, which is one of the main challenges in VLC beamsteering, especially in mobile scenarios.* This requires accurate user positioning, for which visible light positioning (VLP) could be a promising solution. Secondly, *highly dynamic beams affect the illumination functionality, which is harmful for the users in the network.*

To overcome aforementioned challenges, in this work, we propose *BlendVLC*, a cell-free integrated VLC/VLP architecture consisting of two networking planes: 1) a *static plane* composed of *fixed TXs* with immutable beam orientations in a cell-free architecture in which multiple TXs serve one user, and 2) a *dynamic plane* consisting of *steerable TXs* that support beamsteering. This allows to create blended beamspots, originating from both fixed and steerable TXs. A beamspot at a user is defined as the aggregate signal (i.e., aggregate light spot) from the TXs assigned to that user. We tackle the beam tracking problem by performing VLP with the static plane. As the architecture of BlendVLC is inherently cell-free, there are no cell boundaries during downlink transmission, and multiple TXs in the network can cooperate to jointly serve the receivers (RXs) in a user-centric fashion. Since users are allowed to dynamically associate with multiple TXs within their field of view (FoV), BlendVLC could greatly improve the mobility robustness compared to the conventional small cell-based designs [6]. Further, BlendVLC can achieve comparable or even superior performance as a network with more densely placed fixed TXs.

The contributions of this work are summarized as below:

- We propose BlendVLC, a cell-free network architecture empowered by beamspot blending. In BlendVLC, a static plane clusters and localizes the users. Another dynamic plane, in which the TX beams are steerable, uses the real-time positions of users for efficient beamspot blending. The static and the dynamic planes, together, perform data transmission to the users through the blended beamspots. We translate this two-plane network concept into a *building block*, consisting of four fixed TXs and one steerable TX. We show that cooperation between these two planes can boost the system robustness in mobile scenarios.
- We propose a VLP method using a multilayer perceptron neural network to localize the users. Our method achieves an average positioning accuracy of 3.4 cm within 0.45 ms.
- We design a scalable heuristic to blend the TX beamspots in real-time and with low complexity. It improves the system mobility robustness and also works in large networks.
- We carry out extensive experiments in a proof-of-concept testbed to evaluate the system performance of BlendVLC.

We demonstrate that BlendVLC achieves superior performance under various network sizes and topologies.
- We show that our building block is a modular and scalable design that performs well in large networks. For example, in a large network with 21 building blocks, BlendVLC improves the system throughput by 30% compared to a denser network that has *twice* the number of fixed TXs.

II. Background and Design Goals

A. Background

Channel propagation. The intensity of the light beam from an LED is modelled by the Lambertian pattern. Since VLC is line-of-sight (LoS) dominated, it is sufficient to solely consider the LoS propagation. The channel gain h is modelled as:

$$h = \begin{cases} \frac{(m+1)A}{2\pi d^2}\cos^m(\phi)g(\psi)\cos\psi, & 0 \le \psi \le \Psi_c \\ 0, & \text{otherwise} \end{cases}, \quad (1)$$

with m the LED's Lambertian order, A the photodiode's sensing area, d the distance between the TX and RX, ϕ and ψ the irradiation and incidence angles, respectively, $g(\psi)$ the concentrator and filter gain, and Ψ_c the RX's FoV.

Operation modes of LED TXs. Each TX has two operating modes: *1) Illumination mode,* in which the TX is only used for illumination, achieved by applying a constant current through the LED. *2) Illumination+communication mode,* in which the LED is modulated to transmit data. To avoid flickering, the average LED illuminance is the same as in *illumination mode*.

Cell-free VLC and synchronization. In cell-free networking, a *central processing unit (CPU)* coordinates all TXs to form beamspots to desired RXs. For each beamspot, relevant TXs are synchronized via none-line-of-sight (NLOS) VLC [7], [8]. That is, for each RX, the CPU appoints a leading TX from those that will jointly serve the RX. This leading TX transmits a pilot signal that is reflected by the floor, which then can be detected by other TXs to perform synchronization. Then, these TXs jointly send synchronized signals to the desired RX.

B. Design goals

The goal in this work is to design and implement a practical beamspot blending system that addresses following challenges:

Mobility robustness. Highly dynamic TXs face difficulties to ensure a guaranteed stable quality of service to mobile users, as an error in the beam tracking or steering can severely impact the performance. Thus, *the tracking should be accurate, fast and stable over time*. Further, *in case of any error, the system should be able to fall back on a baseline network*, which works independently of the beam tracking and steering.

Fast adaptation. To keep track of mobile users and properly assign the TXs, timely execution of following elements should be assured. Firstly, periodic measurements must be carried out to avoid outdated channel information. Secondly, assigning the TXs and identifying the best steering angle must be performed in real-time with a low-complex method. Finally, the beamspot blending needs to be carried out in a swift manner.

Illumination functionality. Abrupt changes in beamspot blending must be avoided, as they degrade the user experience.

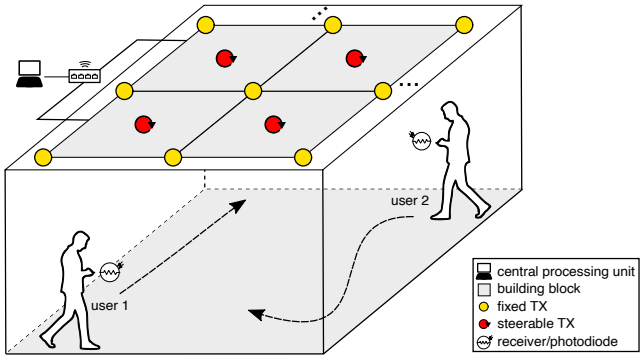

Fig. 1: The system architecture of BlendVLC.

Scalability. To facilitate widespread adoption in large practical networks, the system design should be scalable.

III. System Architecture

We consider an indoor cell-free VLC network with N TXs distributed in a grid on the ceiling and M randomly distributed mobile users. The system architecture is presented in Fig. 1. The network is partitioned in overlapping *building blocks*, each consisting of four fixed TXs and one steerable TX, as detailed further in Sec. III-B. Each TX contains an LED which is used for both illumination and downlink communication, while each user adopts a photodiode to receive data from the TXs. The uplink communication can be based on WiFi or infrared light (IR), as adopted in our system and LiFi-XC [9], respectively. All TXs are connected to a CPU via Ethernet. The CPU manages the cell-free network, partitions nearby users into clusters to avoid excessive inter-user interference, and orchestrates the TX assignments. We consider a multi-user multiple-input-single-output (MU-MISO) scheme, in which a user can be served by multiple synchronized TXs. In this way, one or more *beamspots* can be generated at users, in which a beamspot is defined as the aggregate signal (i.e., aggregate light spot) from the TXs assigned to that user. As the beamspots are small, multiple users can be served in parallel.

A. Networking planes

Static networking plane. This plane consists of fixed TXs, which act as a *baseline network* and provide illumination. *The beam orientations of fixed TXs are immutable and thus do not change over time*. This plane groups nearby users into clusters and provides wireless connectivity to them. Besides, it localizes the users with a novel VLP method, being fundamental for the operation of the dynamic networking plane.

Dynamic networking plane. Based on the user position information from the static plane, the dynamic plane identifies the optimal beam angles of steerable TXs. Then, *it steers these beams to blend with the beamspots from the fixed TXs*, in order to boost the data rate to the users in the network.

Cooperation among these two networking planes allows to create ***blended beamspots****, which are defined as the aggregate light spot originating from combining the signal of both fixed TXs and steerable TXs.* This requires inter-TX synchronization, which is handled as described in Sec. II-A.

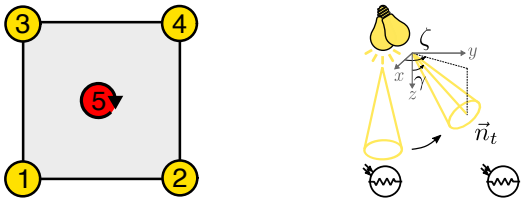

(a) Layout of the building block (b) TX beamsteering

Fig. 2: Illustration of the proposed building block, consisting of four fixed TXs and one steerable TX.

B. System model

The building block. The scalable network architecture consists of overlapping building blocks. Each building block has four fixed TXs and one steerable TX. Its topology is illustrated in Fig. 2a. Each TX can operate in either illumination mode or illumination+communication mode (cf. Sec. II-A). We fix the electrical transmission power budget per area P_a and divide it over the TXs such that the transmission power per TX equals $P_t = (P_a\, A_e)\,/N$, with A_e the area of the environment. The fixed TXs are deployed in a grid with an inter-TX distance Δ_t. Their Lambertian order m, which is related to the half power semi-angle ϕ_{fix} via $m = -1/\log_2(\cos\phi_{\text{fix}})$, is set such that the received signal strength (RSS) at the RX right under the TX is identical for different TX densities Δ_t, i.e., $(m+1) \sim 1/\Delta_t^2$. The steerable TXs have a half power semi-angle ϕ_{steer} and a variable orientation, for which an illustration is depicted in Fig. 2b. The azimuth angle $\zeta \in [0°, 360°]$ represents the angle between the orthogonal projection of the orientation vector $\vec{n}_t$ onto the XY-plane and the positive direction of the X-axis. The polar angle $\gamma \in [0°, 90°]$ denotes the angle between $\vec{n}_t$ and the positive direction of the Z-axis.

Mobile users. We use the random waypoint (RWP) model, a widely adopted mobility model in wireless networks [10], for the trajectories of mobile users. In this model, users first choose their destination randomly in the area. Then, they move along their trajectories on a straight line from the source to the destination at a constant pace. In this work, we set the maximum speed to $v_{max} = 1.4$ m/s and let users move in the area with a random speed between $[v_{max}/2, v_{max}]$ m/s [11]. To reflect realistic scenarios, we add an extra constraint to the model to guarantee a 30 cm minimal inter-user distance.

SINR. To keep track of the cluster a user belongs to, we use the user-cluster vector $\boldsymbol{u} = [u_j] \in \{0, \ldots, C\}^{M\times 1}$, in which u_j denotes the cluster number of RXj and C the number of clusters. Then, the received signal-to-interference-plus-noise ratio (SINR) at RXj can be calculated as follows:

$$\text{SINR}_j = \frac{\left(\rho\,\eta\,P_t \sum_{i=1}^{N} s_{i,u_j}\, h_{i,j}\right)^2}{P_n + \sum_{\substack{c=1\\ c\neq u_j}}^{C} \left(\rho\,\eta\,P_t \sum_{i=1}^{N} s_{i,c}\, h_{i,j}\right)^2}, \quad (2)$$

with ρ the responsitivity of the photodiode, η the wall-plug efficiency of the LED (i.e., the energy conversion efficiency from electrical to optical power), $\boldsymbol{S} = [s_{i,c}] \in \{0,1\}^{N\times C}$ the serving matrix, in which $s_{i,c}$ indicates whether TXi is serving cluster c and with P_n the noise power.

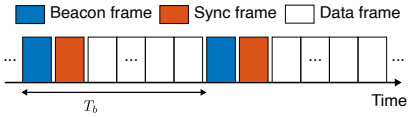

Fig. 3: Illustration of beamspot interval, consisting of a beacon frame, a synchronization frame and multiple data frames.

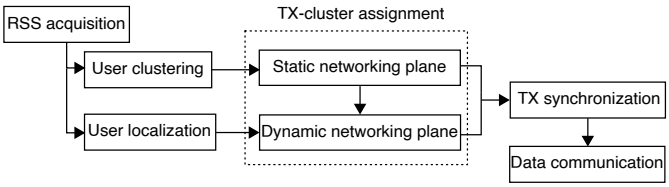

Fig. 4: Flow diagram of BlendVLC.

The achievable throughput R_j at RXj is modelled as below:

$$R_j = \frac{1}{|\mathcal{M}_{u_j}|} B\, \log_2(1 + \text{SINR}_j), \quad (3)$$

with B the communication bandwidth and $|\mathcal{M}_{u_j}|$ the number of RXs in the cluster of RXj. We use $\mathcal{M}_c$ further in this work to denote the set of users in cluster c.

IV. BlendVLC Design

In this section we present the design details of BlendVLC.

A. System workflow

Since the mobile users are subject to a varying channel over time, the channel is measured frequently to avoid performance loss due to outdated information. That is, the time is divided into periodically recurring *beamspot intervals* of duration T_b, as shown in Fig. 3. Each beamspot interval starts with a beacon frame which is used by the CPU to advertise the presence of TXs, by users to measure their downlink channels, and by the CPU to update the resource management of the network. It is followed by a synchronization frame to align the serving TXs and multiple subsequent data frames. The length of the interval must be chosen sufficiently small such that the channel to the mobile users can be assumed approximately unchanged within the interval. It is usually in the range of 100 ms-1000 ms [12]. In every interval, following steps are taken, as shown in Fig. 4.

Step 1: User localization and clustering. After transmission of the beacon frames by the fixed TXs, all users measure the RSS between the fixed TXs and themselves and send this information back to the CPU via the uplink channels. Based on the RSS values, the static networking plane determines the position of the users with VLP using a neural network, for which the details will be presented in Sec. IV-B. Further, the RSS is used by the CPU to group closely spaced users into clusters. That is, users having the same best fixed TX form a cluster (i.e., TX with maximal signal strength to users), for which the CPU appoints this best TX as the master TX for that cluster. Users in different clusters are served in parallel; in case multiple users are in the same cluster, they are served based

on a contention–free time-division multiple access scheme, in which the data frames are equally distributed among the users to ensure user fairness.

Step 2: TX assignments and beamspot blending. Next, the CPU assigns TXs to the clusters. First, the optimal serving TX set is determined for the static networking plane. Then, the CPU determines the optimal assignment of the steerable TXs, as well as their optimal orientations. The serving fixed TXs and steerable TXs, together, generate the blended beamspots and transmit data to the users. Before starting the data transfer, all the serving TXs for a given cluster are first synchronized (cf. Sec. II-A). Then, they jointly transmit synchronized signals to the users in the clusters through the blended beamspots.

Step 3: Blended beamspot operation. Once the steerable TXs are assigned to a cluster and their beam orientations are determined, they keep the orientations fixed during the entire beamspot interval, i.e., they do not change their orientations when switching between users in the same cluster. Firstly, this reduces the delay, as every orientation update requires a settling time, which is around 5 ms when using a micromirror [13]. Secondly, in order to avoid the flickering effect for the human eye, rapid orientation changes above 200 Hz should occur, which is not feasible if the settling time is 5 ms [14].

In the rest of this section, we will answer the following two key questions in designing BlendVLC: *1) how to localize the users and thus support beam tracking and beamspot blending, independent of the network architecture, and 2) how to assign the fixed TXs and the steerable TXs, and find the optimal beam direction of the steerable TXs, to form the blended beamspots?*

B. RSS-based localization with visible light

Based on the channel measurements in the static networking plane, the position of the users can be determined. In this work, we propose a VLP system that applies a *multilayer perceptron (MLP) neural network* to estimate the user positions based on the RSS of downlink channel measurements. *The model does neither require knowledge about the TX arrangement nor about the irradiation pattern of the LEDs; it directly translates the RSS values of the fixed TXs to the 2D coordinates of the users.* The MLP network consists of an input layer, four fully connected hidden layers and an output layer. The output of layer k can be represented as:

$$y_k = f_k\left(\boldsymbol{W}_k\, y_{k-1} + \boldsymbol{b}_k\right), \quad k = 1, \ldots, 5, \tag{4}$$

in which $\boldsymbol{W}_k$ is the weight matrix, f_k the non-linear activation function in layer k, and $\boldsymbol{b}_k$ a bias vector used in layer k. The four hidden layers contain 256, 512, 1024, and 512 neurons, respectively. Thus, the sizes of $\boldsymbol{W}_k$ in the first layer and the last layer are $256 \times N$ and 2×512, respectively. The hidden layers use the LeakyRelu activation function [15], whereas the output layer uses the Sigmoid activation function [16].

To train the model, a data set is constructed through experimental measurements (cf. Sec. VI-A). This data set consists of the RSS values of all fixed TXs in the network and the ground truth positions. The set is randomly split into a training set to train the model, a validation set to tune the hyperparameters

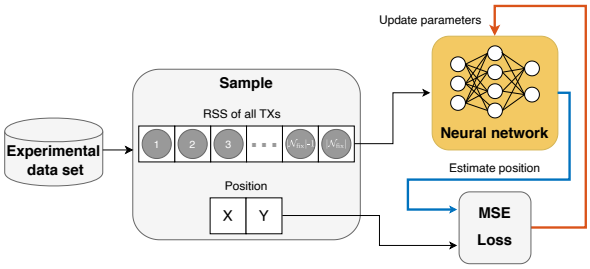

Fig. 5: Overview of the proposed RSS-based VLP empowered by an multilayer perceptron (MLP) neural network.

(e.g., model weights and training batch size), and a test set for final evaluation. An overview of the training procedure is shown in Fig. 5. First, a batch of 32 training samples is loaded from the data set. The RSS values of this batch are forwarded through the network, providing predictions of the position as output. The predictions are compared against the ground truth positions with the mean squared error (MSE) loss function, which corresponds to the euclidean distance between positions. The calculated loss is then used to update the model weights using backpropagation and the Adam optimizer with a learning rate of 10^{-4} [17], improving the model in predicting the positions of the next batch. The model weights are initialised using the initialisation in [18]. To avoid overfitting, early stopping is used, in which the training process is stopped when no performance improvements on the validation set have been observed for 25 epochs. At test time, a new unknown data sample is fed through the network with the trained hyperparameters, and a 2D position estimate is obtained.

C. Beamspots blending

In this section, we present our beamspots blending method, in which a subset of the TXs performs beamsteering and thus adapts their orientation dynamically based on the position of the users in the network. The goal is to optimize the steerable TX's orientation such that the sum of the logarithmic user throughput is maximized, ensuring fair distribution of the user data rates. Since this problem is non-convex and hence gradient based methods can be stuck in local optima, the authors in [14] solve it with a grid-based search method, in which the polar and azimuth angle of the steerable TX is discretized into small sampling intervals and the optimal values are found by testing all combinations. Due to this brute-force search, the complexity scales quadratically with the resolution of the interval and exponentially with the number of steerable TXs.

To get more insight in the system, we propose a two-step approach in which we decouple the cluster assignment from the beam angle adaptation. In the first step, every fixed and steerable TXi is assigned to the optimal cluster $\bar{a}_i$. We start by assigning the set of fixed TXs $\mathcal{N}_{\text{fix}}$ such that:

$$\bar{a}_i = \arg\max_c \sum_{j \in \mathcal{M}_c} \log\left(R_j\right), \quad \forall i \in \mathcal{N}_{\text{fix}}, \tag{5}$$

subject to:

$$\max_c n(c) <= \nu, \tag{6}$$

in which $n(c)$ represents the number of cooperating fixed TXs to cluster c and ν the maximal degree of cooperation. We set ν to the number of fixed TXs in the building block, i.e., $\nu = 4$ for our design. Then, we assign the steerable TXs $\mathcal{N}_{\text{steer}}$, assuming they would be oriented towards the mean position of the users within the cluster[1]:

$$\boldsymbol{p}_c = \frac{1}{|\mathcal{M}_c|} \sum_{j \in \mathcal{M}_c} \boldsymbol{p}_j^r \tag{7}$$

$$\zeta_i = \text{atan2}\left(p_{i,y}^t - p_{c,y}, p_{i,x}^t - p_{c,x}\right) \tag{8}$$

$$\gamma_i = \text{atan2}\left(\sqrt{\left(p_{i,x}^t - p_{c,x}\right)^2 + \left(p_{i,y}^t - p_{c,y}\right)^2}, p_{i,z}^t - p_{c,z}\right) \tag{9}$$

$$\bar{a}_i = \arg\max_{c} \sum_{j \in \mathcal{M}_c} \log\left(R_j\right), \quad \forall i \in \mathcal{N}_{\text{steer}}, \tag{10}$$

subject to:

$$\gamma_{i,min} \leq \gamma_i \leq \gamma_{i,max}, \tag{11}$$

in which $\boldsymbol{p}_i^t$ denotes the position of TXi, $\boldsymbol{p}_j^r$ the position of RXj and $\boldsymbol{p}_c$ the mean RX position in cluster c. The constraint limits the polar angle range of the steerable TXs and thus the set of clusters two which the steerable TXi can be assigned. Throughout this work, we set $\gamma_{min} = 0°$ and γ_{max} such that the steerable TX can maximally be tilted to the farthest location in the coverage region of adjacent fixed transmitters:

$$\gamma_{max} = \arctan\left(\frac{\sqrt{2}\,\Delta_t}{p_{i,z}^t - p_{j,z}^r}\right), \tag{12}$$

in which $p_{i,z}^t$ and $p_{j,z}^r$ is identical for every TXi and RXj, respectively. Given the structure of the proposed building block, this means that the steerable TX can be oriented towards the coverage area of the four adjacent fixed TXs.

In the second step, the orientation of the steerable TX is further optimized within each cluster. In particular, the optimal azimuth angle $\bar{\zeta}_i$ and polar angle $\bar{\gamma}_i$ of steerable TXi is determined as follows:

$$\bar{\zeta}_i, \bar{\gamma}_i = \arg\max_{\zeta_i, \gamma_i} \sum_{j \in \mathcal{M}_{\bar{a}_i}} \log\left(R_j\right), \ \forall i \in \mathcal{N}_{\text{steer}}, \tag{13}$$

subject to:

$$\gamma_{min} \leq \gamma_i \leq \gamma_{max}. \tag{14}$$

V. Insights into the Building Block

To get insight in the system design, we focus in this section on a building block with a size of $2\,\text{m} \times 2\,\text{m} \times 2.8\,\text{m}$, including a steerable TX in the middle and four fixed TXs in the corners, with $\Delta_t = 1.0$ m and a semi-angle of $\phi_{\text{fix}} = 15°$. This layout of the building block is shown in Fig. 6. In the rest of this paper, *we denote this layout as* ***B5***. For the steerable TXs, we use a semi-angle $\phi_{\text{steer}} = 10°$, as it shows a higher minimal throughput along the users' trajectories, as shown in Fig. 7.

Throughout this work, we compare B5 with two other fully static building blocks, consisting of 1) a 4-TX network (***S4***) with $\nu = 4$, and 2) a denser 9-TX network (***S9***) with $\nu = 9$. The TX semi-angle and TX transmission power for these networks is determined according to Sec. III-B, using B5 as the baseline (i.e., S4 and S9 have a 25% higher and 44% lower TX transmission power P_t than B5, respectively).

[1] $\text{atan2}(y, x)$ represents the 2-argument arctangent defined as the angle in the Euclidean plane between the positive x-axis and the ray to the point (x, y).

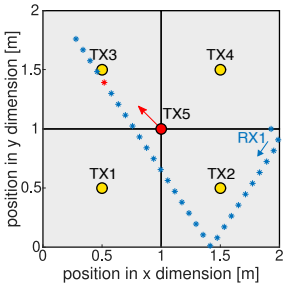

Fig. 6: Building block layout with the red arrow denoting the steerable TX orientation.

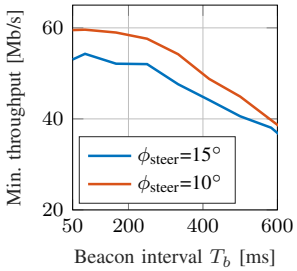

Fig. 7: Impact of semi-angle ϕ_{steer} in building block with $M = 2$.

TABLE I: System parameters.

Parameter	Notation	Value
Noise power	P_n	3.51×10^{-17} W
Bandwidth	B	20 MHz
TX power per area	P_a	0.90 W/m^2
Wall-plug efficiency	η	40%
RX field-of-view, collection area	Ψ_c, A	60°, 1.1 mm^2
RX responsitivity	ρ	0.40 A/W

In this paper, we set the duration of the beamspot interval to $T_b = 100$ ms. This means that with $v_{max} = 1.4$ m/s, users can move at most 14 cm within the interval. As shown in Fig. 7, this ensures a limited loss due to outdated information for the considered TX semi-angles. We analyze the performance by emulating 20 random user iterations with a duration of 3 seconds. Other system parameters are presented in Table I.

A. Comparison of the beamspot blending methods

We compare the performance of the different beamspot blending methods described in Sec. IV-C. To simulate the grid-based method, we divide the area in tiles with 10 cm side length, calculate the channel gain in every tile and obtain the optimal orientation by selecting the best performing one among all tiles. The Cumulative Distribution Function (CDF) of the user throughput for a network with $M = 3$ users is shown in Fig. 8a. First, we observe that the grid-based method results in very similar performance as the two-step approach (labelled '2-step, optimal'). By using the two-step approach, the average time to calculate the assignment and optimal orientation of the steerable TXs can be reduced from 295 ms to 59 ms, a 5× improvement. Next, we conclude that pointing to the mean position of users within the selected cluster (labelled '2-step, mean') instead of optimizing the orientation within the cluster in Eq. (13) results in very similar proportional fairness. This can further reduce the calculation time to 2.5 ms.

Insight 1. Our two-step approach can achieve comparable performance as the exhaustive grid-based method. Optimal

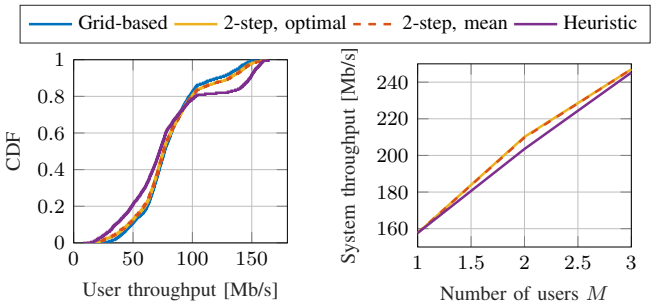

(a) User throughput for $M = 3$ (b) Average system throughput

Fig. 8: Comparison of methods to create blended beamspots in building block network with $M = 1$ to $M = 3$ users.

proportional user fairness can be approximated by steering the beams to the mean user position of the selected cluster.

B. Scalable heuristic

The optimization problem of the two-step approach requires centralized knowledge about all building blocks in the network and its computational complexity scales exponentially in terms of the number of fixed TXs $\sim (C+1)^{|\mathcal{N}_{\text{fix}}|}$ and steerable TXs $\sim 5^{|\mathcal{N}_{\text{steer}}|}$. Therefore, we propose a low-complex heuristic, which performs TX-cluster assignments in a distributed manner and determines the orientation of the steerable TXs independently per building block. That is, we determine the best cluster $\tilde{a}_i$ for a fixed/steerable TXi such that:

$$\beta(c) = \frac{\frac{1}{|\mathcal{M}_c|}\sum_{j\in\mathcal{M}_c} P_s(i,j)}{\frac{1}{|\mathcal{M}\setminus\mathcal{M}_c|}\sum_{j\in\mathcal{M}\setminus\mathcal{M}_c} P_i(i,j)} \tag{15}$$

$$\tilde{a}_i = \begin{cases} \arg\max_c \beta(c), & \beta(\tilde{a}_i) > \tau \\ \emptyset, & \text{otherwise} \end{cases}, \tag{16}$$

with $P_s(i,j)$ the desired signal power from the TXi to RXj if the TX would be assigned to cluster c and $P_i(i,j)$ the interference power generated by TXi to RXj. For the fixed TX, these values can be directly obtained from the channel quality measurements and Eq. (2). For the steerable TX, we concluded that pointing the steerable TXs to the mean user position in the cluster shows comparable performance as optimizing the orientation within the cluster. Therefore, after localizing the users, we use the position information to estimate the channel quality with Eq. (1), assuming the TX points to the mean position in the cluster. This avoids the need for an exhaustive search over all possible orientations of the steerable TX. Further, a fixed/steerable TX is only assigned to a cluster if $\beta(\tilde{a}_i) > \tau$, to enable a TX only if it results in a significant improvement. We found empirically that $\tau = 100$ shows good performance, and therefore is used further in this work. We use the same constraints as before, for the fixed TXs in Eq. (6) and the steerable TXs in Eq. (11).

From Fig. 8a, it is clear that the heuristic achieves comparable performance, although it favors more the higher throughput regime compared to the two-step approach. It can reduce the calculation time to 2.1 ms with a loss of 1% in average user throughput for $M = 3$. Also for other user densities in Fig. 8b, we draw similar conclusions. We emphasize that the heuristic allows distributed TX-cluster assignments and that the best steerable TX orientations can be set locally per building block, making it suitable for large network deployments.

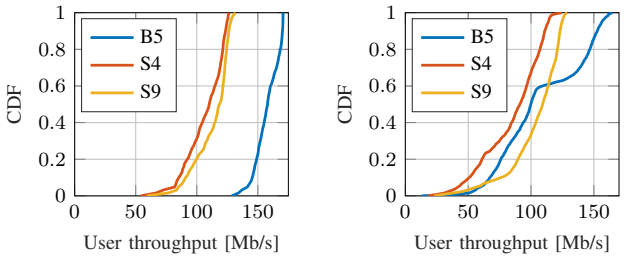

(a) $M = 1$ (b) $M = 2$

Fig. 9: CDF of user throughput in the building block network for BlendVLC (B5) and fully static networks (S4 and S9).

C. Comparison with fully static (denser) networks

We compare the performance of the building block B5 of the BlendVLC with the fully static 4-TX (S4) and 9-TX (S9) networks. The CDF of the user throughput is depicted in Fig. 9. Overall, we observe a clear gain in the user throughput compared to the static networks. If $M = 1$, then there is only a single user in the network such that the maximum ν fixed TXs and the steerable TX can always be assigned to the RX. This leads to a 48% and 39% higher average user throughput compared to S4 and S9, respectively. If $M = 2$, the fixed TXs and steerable TX need to take into account the interference they might generate to other clusters by choosing one cluster. Nevertheless, the B5 can improve the average user throughput with 27% compared to S4. Although S9 can serve more clusters in parallel, B5 still shows a slight improvement of 1.3% in user throughput.

Insight 2. BlendVLC can achieve comparable (S9) or even superior (S4) performance compared to fully static networks, for the same total transmission power.

D. Cluster switching interval

Adapting the orientation of TXs alters the illumination pattern, which can result in temporal light artefacts such as flicker [19]. We empirically observe from our experimental evaluation that most abrupt changes occur when the steerable TXs switch between clusters. Therefore, we aim to extend this *cluster switching interval*, by adding an extra constraint to Eq. (10) to ensure a new cluster is only selected on the condition that the gain in proportional fairness due to switching compared to the current cluster is higher than a predefined threshold. Otherwise, the TX keeps its cluster while still having the ability to update its orientation within the cluster. Next to reducing the switching frequency, this has also the advantage of requiring less frequent re-synchronization among the TXs serving the same cluster. The impact on the user throughput is shown in Fig. 10a. We observe that without constraint, the average switching interval is around 0.5 s. By

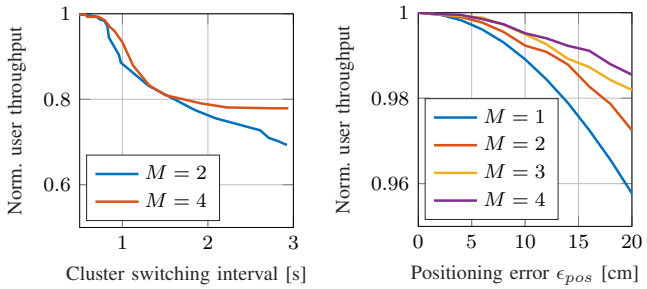

(a) Cluster switching (b) Positioning error

Fig. 10: Impact of cluster switching and positioning error.

adding the constraint, the switching interval can be enlarged to 1.5 s while keeping 80% of the maximal user throughput. Further, we see that the more users in the network, the lower the sensitivity as it is more likely that another user can benefit from the steerable TX.

Insight 3. Most abrupt illumination changes occur between cluster switches, which can be reduced by switching only if the gain in performance is significant.

E. Impact of positioning error

We showed that pointing the steerable TX towards the mean user position in the cluster achieves good performance. To study the impact of errors in the estimated positions, we add a random vector $\tilde{\boldsymbol{p}}$ to $\boldsymbol{p}_j^r$, the real position vector of RXj, such that the euclidean distance equals the positioning error ϵ_{pos}:

$$\left\| \left(\boldsymbol{p}_j^r + \tilde{\boldsymbol{p}} \right) - \boldsymbol{p}_j^r \right\|_2 = \epsilon_{pos}. \tag{17}$$

We focus on 2D localization errors, i.e., $\tilde{p}_z = 0$. The result is shown in Fig. 10b for $\phi_{\text{steer}} = 10°$ in a network up to $M = 4$ users. We conclude that BlendVLC is robust against position errors. For $\epsilon_{pos} < 10$ cm, the average user throughput drops at most 1.1%. Further, we note that the more users in the network, the higher the resilience against localization errors. This is because calculating the average position in a cluster averages out the positioning error, reducing its impact.

Insight 4. BlendVLC is robust against errors in the estimated user positions, especially for larger user densities.

VI. Performance Evaluation

In this section, we evaluate the performance of BlendVLC with extensive experiments.

BlendVLC implementation. We use the open-source TX and RX front-end provided in [7], [8] as a basis for our implementation of the fixed TXs and users. For the steerable TXs, we leverage two TowerPro SG90 servo motors to control the azimuth and polar angle of the steerable TXs, to perform beamsteering. This solution is very low cost ($7). Our implemented proof-of-concept BlendVLC is shown in Fig. 11, in which a snapshot of the steerable TX with pan-tilt is given on the right.

Experimental setup. We evaluate the performance by experiments in a network with four overlapping building blocks in an area of $3\text{ m} \times 3\text{ m}$, resulting in total 13 TXs for B5

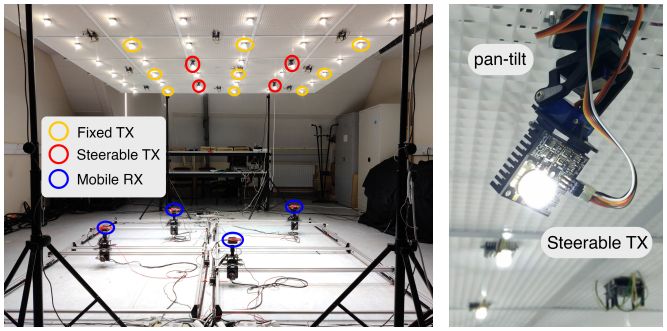

Fig. 11: Our developed proof-of-concept BlendVLC testbed: left) the whole testbed that includes the *fixed TX* whose beams cannot be steered, the *steerable TXs*, and the *mobile RXs* that are controlled by the ACRO systems; right) a *steerable TX*.

and nine TXs for S4 (each having 44% more transmission power P_t than B5). The TXs are located at a height of 192 cm from the floor and have a $\Delta_t = 1.0$ m inter-TX distance. The fixed TXs have a semi-angle $\phi_{\text{fix}} = 15°$. The RXs are placed on the floor at a height of 0.4 m and are controlled by four OpenBuilds ACRO Systems [20] to dynamically adapt their positions in the area. We use the proposed heuristic from Sec. V-B for the TX assignments and beamspot blending. Due to the limitations of the proof-of-concept testbed in adapting the inter-TX distance and the TX semi-angle, we investigate B5 and S4 in experiments while analyzing the denser static network with S9 (25 TXs with 48% smaller P_t than B5) in a *simulator* that we develop in Matlab.

A. RSS-based positioning with light

First, we evaluate the performance of our VLP method in the experimental setup with four building blocks. To construct the data set, we traverse the spatial coverage area of the ACRO systems in steps of 1 cm. This leads to 121 steps in the X and Y direction for every ACRO system. We take three channel measurements from the nine fixed TXs for every position. Further, we consider two different heights of the ceiling, one at a height of 176 cm and the other at 192 cm. This results in a total data set of 351384 samples, in which 64% is used for the training set, 16% for the validation set and 20% for the test set. Training is performed using the PyTorch framework for a duration of about two hours. To evaluate the performance, we use the euclidean distance between the real position and the estimated position as the metric of interest.

On the test set, the position of the users can be determined with an average accuracy of 3.4 cm within 0.45 ms. To get more insight in the spatial error distribution, we analyze a 2D heatmap, which contains a sample for every possible 2D location in the grid and thus consists of a mix of training, validation and test set. The result is shown in Fig. 12. Since not all locations are accessible by the ACRO systems, a cross-like shape is visible in the figure. The average 2D accuracy on the heatmap equals 3.7 cm. We conclude that our VLP system achieves a high accuracy and ensures a minimal loss in user throughput of less than 1%, as indicated before in Fig. 10b.

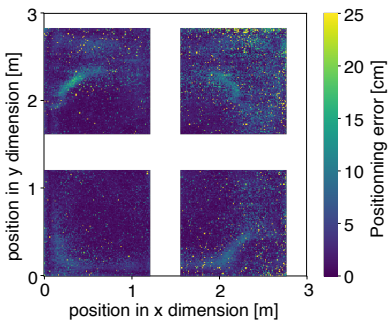

Fig. 12: Heatmap of positioning errors from experiment (*the cross-like area is not accessible by ACRO*).

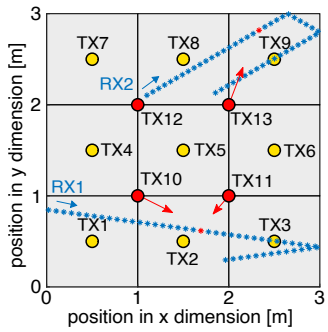

Fig. 13: Illustration of a random trajectory in a 4-building block network with $M = 2$.

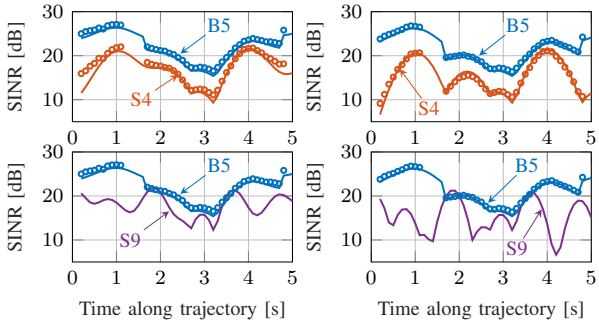

(a) With cooperation (b) Without cooperation

Fig. 14: SINR for RX2 along the trajectory in Fig. 13. Circles: experiments; solid lines: simulations.

B. Cell-free networking

1) Comparison with fully static (denser) networks: We first consider an instance with $M = 2$ users whose trajectories are depicted in Fig. 13. When moving along the trajectories with the ACRO systems, the users measure the channel qualities and calculate the SINR according to Eq. (2). With the SINR values as inputs, the user throughput is obtained using Eq. (3). We investigate both the configurations with and without cooperation among fixed TXs ($\nu = 1$, i.e., a single fixed TX is assigned to a cluster). As an example, we show the experimental SINR of RX2 in Fig. 14. With cooperation, an average SINR of 22.1 dB is achieved with the B5 building block of BlendVLC, compared to 17.7 dB and 18.2 dB in a fully static network with the S4 and S9 building block, respectively. This means that B5/BlendVLC realizes an improvement of 4.4 dB and 3.9 dB, respectively. Without cooperation, we note an increase in average SINR of 6.1 dB and 5.8 dB compared to S4 and S9. This gain is higher because without cooperation S4 and S9 can only assign a single TX to the selected cluster, whereas B5/BlendVLC might also assign the steerable TXs in addition to a fixed TX. We note that some experimental measurements are missing in Fig. 14. This is because not all positions within the area are accessible by the ACRO systems (cf. Fig. 12). Further, we provide the evaluation results from our simulator, as shown by the solid lines in Fig. 14. We can observe a good match between the experimental results and the simulation results. The little deviations are due to the fact that the servo motors of the steerable TXs are not responsive to very small angle updates because of hardware inaccuracies.

To generalize these results, we perform measurements for 10 random trajectories in a network with $M = 2$. We analyze the CDF of the user throughput both with and without cooperation among fixed TXs. The result is shown in Fig. 15. We observe a clear improvement of B5/BlendVLC compared to S4. The experimental average user throughput increases from 121 Mb/s to 145 Mb/s with cooperation, and from 104 Mb/s to 138 Mb/s without cooperation. That is, B5/BlendVLC shows a gain of 19% and 33%, respectively. From the figures, the gain compared to S9 is also clearly visible. As above, the gain without cooperation is higher because B5/BlendVLC has the ability to assign steerable TXs in addition to fixed TXs.

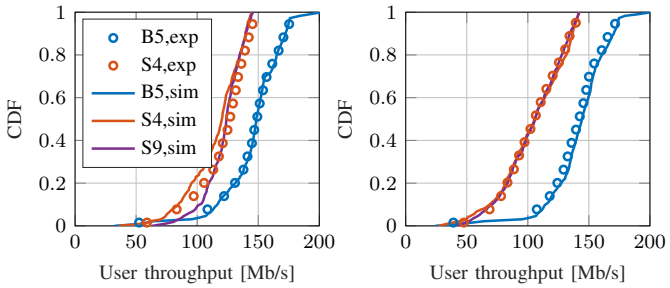

(a) With cooperation (b) Without cooperation

Fig. 15: CDF of experimental user throughput for BlendVLC (B5) and fully static networks (S4 and S9) for $M = 2$.

2) Corridor evaluation: We also evaluate the performance of BlendVLC in a realistic corridor scenario consisting of two B5 building blocks, as depicted in Fig. 16. As before, we compare the performance with the fully static networks, in which now each TX has a 33% more (S4) and 47% lower (S9) transmission power compared to B5. Due to space limitations, we only show the results with cooperation among fixed TXs. The exemplary trajectories for $M = 1$ and $M = 2$ users are shown in Fig. 16a and 16b, respectively. The experimental result for the trajectory in Fig. 16a is shown in Fig. 17a. We observe that B5 achieves a gain of 23% in the experimental average user throughput and a similar improvement of 27% compared to S9 in simulations. Fig. 16b shows the trajectories of two users in the corridor moving in opposite directions. The average user throughput is depicted in Fig. 17b, for which B5 improves the user throughput by 21%, both compared to S4 in the experiment and S9 in the simulation.

C. Emulation in larger-scale networks

Lastly, we evaluate BlendVLC in a larger-scale conference room with an area of $8\,\mathrm{m} \times 4\,\mathrm{m}$. This room consists of 21 overlapping building blocks, leading to a total number of 53 TXs for B5, 32 TXs for S4 and 105 TXs for S9. The users can move freely and we vary the number of users from one to 12. The evaluation is done in the simulator because we do not have enough TXs and RXs in the lab. We consider 20 random trajectories of the users, with a minimal inter-user distance of 20 cm and a duration of 7.5 seconds per trajectory.

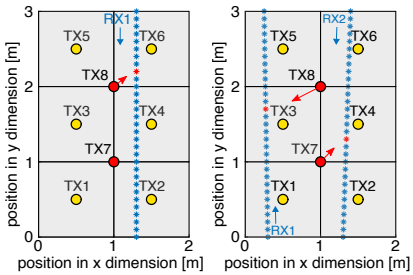

(a) $M = 1$ (b) $M = 2$

Fig. 16: Experimental setup (incl. user trajectories) of the corridor scenario.

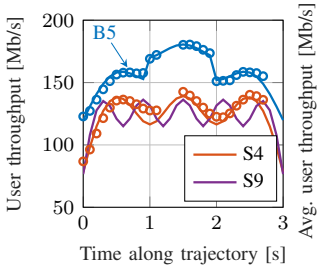

(a) $M = 1$

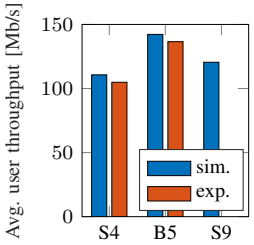

(b) $M = 2$

Fig. 17: Evaluation results of the corridor scenario. Circles: experiments; solid lines: simulations.

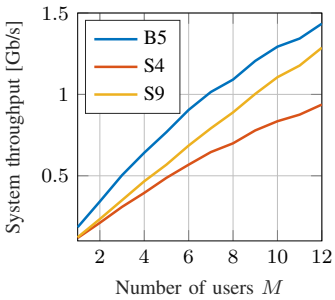

Fig. 18: Evaluation in a network with 21 building blocks.

The evaluation results are shown in Fig. 18. We observe that B5/BlendVLC achieves superior system throughput compared to the fully static networks S4 and S9. The average system throughput over the considered user densities in B5/BlendVLC improves with 57% and 30% compared to S4 and S9, respectively. An important note is that B5/BlendVLC only requires around 50% TXs to be deployed compared to S9.

VII. Discussions

Beamsteering. In our implementation, the beams of TXs are steered mechanically with low-cost pan-tilts, showing already clear performance improvements. Envisioning a more practical system, the pointing precision and adaptation speed could be improved by advanced steering techniques. In general, all techniques face a fundamental trade-off between steering range and granularity. Mechanical gimbals support 360° steering but are imprecise and bulky [21]. They might be combined with fine-grained steering techniques with smaller steering ranges, e.g., a micromirror controlled by a piezoelectric actuator [5] or a micro-electromechanical system [22]. To avoid mechanical movement, a spatial light modulator with liquid crystals can be used, allowing to program reflection or transmission gratings dynamically [23], [24]. Finally, steering beams might be realized with fully passive devices by tuning the wavelength of light in combination with diffractive gratings [25].

Illumination. Adapting the orientation of TXs might impact the illumination distribution [26]. To minimize this, we take two measures. Firstly, we only use a limited set of steerable TXs next to the fixed TXs which provide stable illumination. Secondly, as our experiments show that most abrupt changes occur when steerable TXs switch among clusters, we advise TXs to only switch when the resulting gain is significant. To provide fully stable illumination, we argue that the steerable TXs can use infrared light instead of visible light. By designing a receiver front-end that is sensitive to both visible and infrared light, an integrated flicker-free system can be realized.

Localization. Extensive research exists on the localization using visible light [27]. Our work in particular focuses on an RSS-based neural network technique with densely deployed TXs that has not been studied before. In our future work, we will compare its performance to state-of-the-art VLP methods.

VIII. Related work

We summarize the most relevant works in this section.

Beam tracking. Beam tracking has been extensively studied in free-space optical communications [21], which is one of the main challenges in beamsteering [28], [29] and can result in delays in the order of seconds [30]. The authors in [31] propose an accurate beam alignment algorithm for inter-vehicular laser communication, in which they use a sensor control loop running at 1 KHz, introducing non-negligible overhead. This challenge also exists in mmWave communications due to the highly directional antennas, for which various solutions are proposed [32], [33], including accurate positioning techniques based on light to reduce the tracking complexity [34], [35].

Beamsteering. The work in [4] studies the benefits of beamsteering in VLC, focusing on the illumination functionality. In [5], a SINR gain of 12 dB in the low region is achieved by beamsteering. Further, the same authors optimize the steering angles in a single TX network with multiple beams to maximize user throughput [14]. However, they neither address the beam tracking challenge nor study user mobility. In [26], [36] the application of holograms in VLC beamsteering is reported, in which an algorithm is proposed to reduce the time needed to determine the optimal beam angle and generate the hologram. By deploying steered narrow infrared laser beams, the authors in [25] build a system achieving Gb/s links to multiple users which are localized with corner cube reflectors.

In contrast to BlendVLC, none of the above related works consider a fully integrated system that provides both accurate positioning and beamsteering based on visible light. Further, all the TXs are assumed to be steerable, whereas we consider a modular building block with a subset of steerable TXs, which reduces the cost and makes it scalable for large networks.

IX. Conclusion

We have designed BlendVLC, a cell-free network architecture that improves mobility robustness of users by beamspot blending. BlendVLC provides an integrated solution, tackling both the beam tracking and steering challenges. We designed an accurate VLP technique empowered by a neural network. Based on that, we proposed a scalable heuristic for beamspot blending. We demonstrated that BlendVLC achieves superior performance compared to a fully static denser network.

Acknowledgment

This work is supported in part by the Research Foundation Flanders SB PhD fellowship under grant number 1S59918N.

REFERENCES

[1] "Cisco Annual Internet Report (2018–2023) - White Paper." [Online]. Available: https://www.cisco.com/c/en/us/solutions/collateral/executive-perspectives/annual-internet-report/white-paper-c11-741490.html

[2] L. Hanzo, H. Haas, S. Imre, D. O'Brien, M. Rupp, and L. Gyongyosi, "Wireless myths, realities, and futures: From 3G/4G to optical and quantum wireless," *Proceedings of the IEEE*, 2012.

[3] C. Chen, D. A. Basnayaka, and H. Haas, "Downlink performance of optical attocell networks," *IEEE Journal of Lightwave Technology*, 2016.

[4] M. B. Rahaim, J. Morrison, and T. D. C. Little, "Beam control for indoor FSO and dynamic dual-use VLC lighting systems," *Springer Journal of Communications and Information Networks*, 2017.

[5] Y. Said Eroglu, I. Guvenc, A. Sahin, N. Pala, and M. Yuksel, "Diversity Combining and Piezoelectric Beam Steering for Multi-Element VLC Networks," in *Proceedings of the ACM Workshop on Visible Light Communication Systems (VLCS)*, 2016.

[6] R. Jiang, Q. Wang, H. Haas, and Z. Wang, "Joint User Association and Power Allocation for Cell-Free Visible Light Communication Networks," *IEEE Journal on Selected Areas in Communications*, 2018.

[7] J. Beysens, A. Galisteo, Q. Wang, D. Juara, D. Giustiniano, and S. Pollin, "DenseVLC: a cell-free massive MIMO system with distributed LEDs," in *Proceedings of ACM International Conference on emerging Networking EXperiments and Technologies (CoNEXT)*, 2018.

[8] J. Beysens, Q. Wang, A. Galisteo, D. Giustiniano, and S. Pollin, "A Cell-Free Networking System With Visible Light," *IEEE/ACM Transactions on Networking*, 2020.

[9] "LiFi-XC." [Online]. Available: https://lifi.co/lifi-products/lifi-xc/

[10] C. Bettstetter, H. Hartenstein, and X. Costa, "Stochastic Properties of the Random Waypoint Mobility Model," *Springer Wireless Networks*, 2004.

[11] M. Soltani, A. Purwita, Z. Zeng, H. Haas, and M. Safari, "Modeling the Random Orientation of Mobile Devices: Measurement, Analysis and LiFi Use Case," *IEEE Transactions on Communications*, 2018.

[12] T. Nitsche, C. Cordeiro, A. Flores, E. Knightly, E. Perahia, and J. Widmer, "IEEE 802.11ad: Directional 60 GHz Communication for Multi-Gigabit-per-Second Wi-Fi," *IEEE Communications Magazine*, 2014.

[13] J. Morrison, M. Imboden, T. D. Little, and D. J. Bishop, "Electrothermally actuated tip-tilt-piston micromirror with integrated varifocal capability," *OSA Optics Express*, 2015.

[14] Y. Said Eroglu, C. K. Anjinappa, I. Guvenc, and N. Pala, "Slow Beam Steering and NOMA for Indoor Multi-User Visible Light Communications," *IEEE Transactions on Mobile Computing*, 2019.

[15] V. Nair and G. Hinton, "Rectified Linear Units Improve Restricted Boltzmann Machines," in *Proceedings of the International Conference on International Conference on Machine Learning (ICML)*, 2010.

[16] J. Han and C. Moraga, "The influence of the sigmoid function parameters on the speed of backpropagation learning," in *Proceedings of the Springer International Workshop on Artificial Neural Networks (IWANN)*, 1995.

[17] D. P. Kingma and J. Ba, "Adam: A Method for Stochastic Optimization," in *Proceedings of the International Conference on Learning Representations (ICLR)*, 2015.

[18] K. He, X. Zhang, S. Ren, and J. Sun, "Delving deep into rectifiers: Surpassing human-level performance on imagenet classification," in *Proceedings of IEEE International Conference on Computer Vision (ICCV)*, 2015.

[19] "Visual Aspects of Time-Modulated Lighting Systems." [Online]. Available: http://cie.co.at/publications/visual-aspects-time-modulated-lighting-systems-definitions-and-measurement-models

[20] "OpenBuilds ACRO System." [Online]. Available: https://openbuilds.com/builds/openbuilds-acro-system.5416/

[21] Y. Kaymak, R. Rojas-Cessa, J. Feng, N. Ansari, M. Zhou, and T. Zhang, "A Survey on Acquisition, Tracking, and Pointing Mechanisms for Mobile Free-Space Optical Communications," *IEEE Communications Surveys and Tutorials*, 2018.

[22] C. Pollock, J. Morrison, M. Imboden, T. D. Little, and D. Bishop, "Beam shaping with tip-tilt varifocal mirror for indoor optical wireless communication," *OSA Optics Express*, 2017.

[23] A. Gomez, K. Shi, C. Quintana, M. Sato, G. Faulkner, B. C. Thomsen, and D. O'Brien, "Beyond 100-Gb/s indoor wide field-of-view optical wireless communications," *IEEE Photonics Technology Letters*, 2015.

[24] S. Sabouri and K. Jamshidi, "Design Considerations of Silicon Nitride Optical Phased Array for Visible Light Communications," *IEEE Journal of Selected Topics in Quantum Electronics*, 2018.

[25] T. Koonen, K. Mekonnen, Z. Cao, F. Huijskens, N. Pham, and E. Tangdiongga, "Ultra-high-capacity wireless communication by means of steered narrow optical beams," *Philosophical Transactions of the Royal Society A: Mathematical, Physical and Engineering Sciences*, 2020.

[26] A. Hussein, M. Alresheedi, and J. Elmirghani, "Fast and efficient adaptation techniques for visible light communication systems," *OSA Journal of Optical Communications and Networking*, 2016.

[27] Y. Zhuang, L. Hua, and *et al.*, "A Survey of Positioning Systems Using Visible LED Lights," *IEEE Communications Surveys Tutorials*, 2018.

[28] M. T. Alresheedi and J. M. Elmirghani, "Performance evaluation of 5 Gbit/s and 10 Gbit/s mobile optical wireless systems employing beam angle and power adaptation with diversity receivers," *IEEE Journal on Selected Areas in Communications*, 2011.

[29] Z. Vatansever and M. Brandt-Pearce, "Effects of unknown shadowing and non-line-of-sight on indoor tracking using visible light," *Proceedings of the IEEE Military Communications Conference (MILCOM)*, 2017.

[30] A. Gomez, K. Shi, C. Quintana, G. Faulkner, B. C. Thomsen, and D. O'Brien, "A 50 Gb/s Transparent Indoor Optical Wireless Communications Link With an Integrated Localization and Tracking System," *IEEE Journal of Lightwave Technology*, 2016.

[31] M. Brambilla, D. Tagliaferri, M. Nicoli, and U. Spagnolini, "Sensor and Map-Aided Cooperative Beam Tracking for Optical V2V Communications," *Proceedings of IEEE Vehicular Technology Conference (VTC)*, 2020.

[32] H. Hassanieh, M. Abdelghany, O. Abari, D. Katabi, M. Rodriguez, and P. Indyk, "Fast millimeter wave beam alignment," *Proceedings of the ACM Special Interest Group on Data Communication (SIGCOMM)*, 2018.

[33] J. Zhao, F. Gao, L. Kuang, Q. Wu, and W. Jia, "Channel Tracking with Flight Control System for UAV mmWave MIMO Communications," *IEEE Communications Letters*, 2018.

[34] A. M. Nor and E. M. Mohamed, "Li-Fi Positioning for Efficient Millimeter Wave Beamforming Training in Indoor Environment," *Springer Mobile Networks and Applications*, 2019.

[35] M. Haider, Y. Ghasempour, and E. Knightly, "SearchLight: Tracking device mobility using indoor luminaries to adapt 60 GHz beams," *Proceedings of the International Symposium on Mobile Ad Hoc Networking and Computing (MobiHoc)*, 2018.

[36] M. Alresheedi, A. T. Hussein, and J. Elmirghani, "Uplink design in VLC systems with IR sources and beam steering," *IET Communications*, 2017.